STRUCTURE OF HIGH REYNOLDS NUMBER ADVERSE PRESSURE GRADIENT TURBULENT BOUNDARY LAYER

Murat Tutkun[*,] , William K. George[**] , Michel Stanislas[**]**
[*]Norwegian Defence Research Establishment (FFI), P.O. Box 25, 2027 Kjeller, Norway
[**]Laboratoire de Mécanique de Lille, École Centrale de Lille, UMR CNRS 8107,
Bv Paul Langevin, 59655 Villeneuve d'Ascq, France
murat.tutkun@ffi.no; georgewilliamk@gmail.com; michel.stanislas@ec-lille.fr

Keywords: *High Reynolds number, adverse pressure gradient, turbulent boundary layer, hot-wire anemometry, two-point correlations.*

Abstract

A high Reynolds number adverse pressure gradient turbulent boundary layer experiment was carried out in the large wind tunnel of Laboratoire de Mécanique de Lille using synchronized stereo PIV systems and a hot-wire rake of 143 single wire probes. A 2D bump was used to create converging-diverging flow inside the test section. Measurement were performed on the decelerating part of the bump. Reynolds number based on the momentum thickness was 17 100*. In order to investigate structural characteristics of the high Reynolds number turbulent boundary layer under influence of strong adverse pressure gradient in a statistical sense, simultaneously sampled hot-wire data of 143 probes were used to compute two-point correlations on both streamwise – spanwise (XZ) planes parallel to wall and streamwise – wall-normal (XY) planes normal to the wall. The results presented in this paper indicate that most of the activity creating significant correlations is confined from wall to top of the log-layer, which is about* y^+ *of 700 in this case. Maximum streamwise extent of the correlation on XZ plane is approximately* $\pm 4.5\delta$*. Similarly, the elongated correlations in the streamwise direction on XY planes reach maximum* 10δ *in length inside the log-layer. The wake region produces weak correlations compared to the ones observed inside the log-layer.*

1 Introduction

Turbulent boundary layers under influence of adverse pressure gradient (APG) are one of the most common engineering problems present in aerospace, chemical, environmental and energy related industries and therefore of great technical importance. A constant application of APG may lead flow separation which imposes limitation on performance of the devices and increases drag and fuel consumption. In addition, presence of APG may severely affect the lift and thrust when wigs and propellers are considered respectively.

Even though APG turbulent boundary layers have been studied extensively over the years, the problem still lacks a complete understanding of physical mechanisms underlying the complex dynamics. This lack of knowledge adversely affects turbulence modeling strategies used in the industry. Accurate prediction of when and where the separation occurs during the operation is of great importance in designing wings and bodies.

Large and very large scales of motions in turbulent boundary layers have recently received a great deal of attention because of their contribution to turbulence kinetic energy and Reynolds shear stresses[2, 3, 7, 8, 9, 10, 12, 14]. A current state of knowledge on the large scale organized motions, the so-called coherent structures, in wall bounded turbulent flows have recently been documented in detail in [1]. Obvious features of

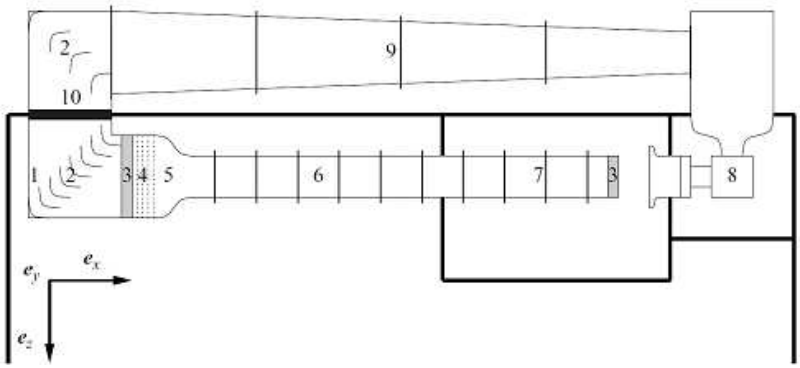

Fig. 1 Schematic of the LML wind tunnel: 1, plenum chamber; 2, guide vanes; 3, honeycomb; 4, grids; 5, contraction; 6, turbulent boundary layer developing zone; 7, testing zone of wind tunnel; 8, fan and motor; 9, return duct; 10, heat exchanger (air−water).

these large scale motions can be observed easily in nature and laboratory environment, however, quantification of these observations is either difficult or impossible in many situations. Multipoint measurements are found to be useful to extract some information regarding the statistical description of the turbulence in these flows. Even though there have been experiments and numerical simulations to study large scale motions in turbulent channel, pipe and boundary layer flows, usually at small or intermediate Reynolds numbers, there certainly is a need for an investigation on first the large and very large scale motion in APG turbulent boundary layers and second the behavior of these scales when the Reynolds number is high.

In this paper, we present experimental multipoint measurements of high Reynolds number turbulent boundary layer subjected to adverse pressure gradient. The paper deals with the two-point correlations obtained from the measurements in order to study statistical description of correlation lengths in both longitudinal, wall-normal and spanwise directions. The data are obtained using a hot-wire rake of 143 single-wire probes, which was synchronized with stereo PIV systems. 143 hot-wire probes were distributed on an array perpendicular to the streamwise flow direction and measured at each point simultaneously. The adverse pressure gradient was created by means a 2D bump placed in the test section of the wind tunnel. The resulting Reynolds number based on momentum thickness at the measurement location was about 17 100.

2 Experimental Setup

An experiment on the turbulent boundary layer under the influence of strong adverse pressure gradient was carried out in the LML wind tunnel of Laboratoire de Mécanique de Lille, France. The LML wind tunnel's test section is 20 m in length, 2 m in width and 1 m in height. The first 15 m of the test section is used for flow development and the last 5 m of that is used as working test section. As shown in Fig. 1, LML tunnel is a closed circuit wind tunnel with a maximum freestream velocity of 10.5 m s^{-1}. Three dimensional roughness elements were used on the bottom wall of the wind tunnel in the entrance of the test section to trip the flow into turbulence quickly. A Pitot tube connected to a Furness micromanometer was used to monitor the constant tunnel velocity, which was achievable with a precision of 0.25%. A uniform operating air temperature was obtained using a temperature control unit placed in the return duct of the tunnel. Further details about the tunnel and its flow quality can be found in [5, 13].

A specially designed 2D bump shown in Fig. 2 was used to obtain the adverse pressure gradient, or decelerating, flow within the test section

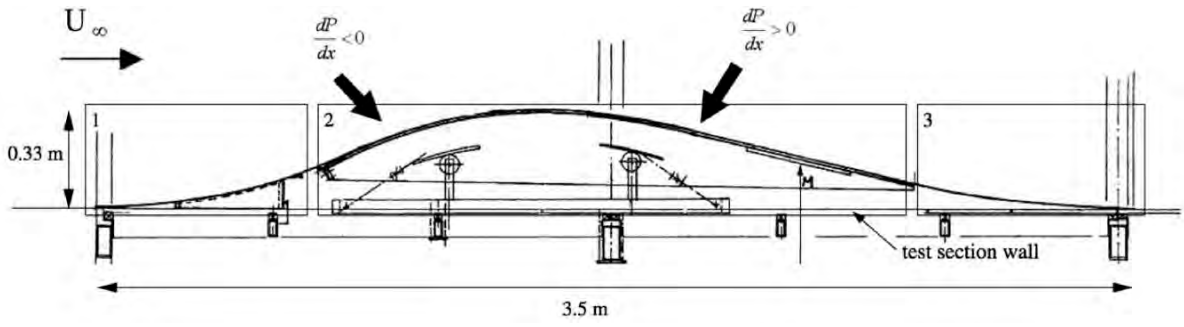

Fig. 2 Schematic of the 2D bump used to create adverse pressure gradient.

of the wind tunnel. This bump was computed and designed by Dassault Aviation to produce a pressure gradient representative of the suction side of airfoil at high angle of attack [4]. Length of the bump in the streamwise direction was 3.5 m and flow in the wind tunnel meets the bump after 15.5 m development inside the test section. The bump reaches it maximum thickness, which is 0.33 m, in 1.5 m in the streamwise direction, corresponding to downstream location of 17 m with respect to inlet of the test section. The boundary layer thickness over the decelerating part of the bump varies between 0.115 m and 0.455 m. The measurements presented in this study were performed 17.90 m downstream of the inlet, which resulted in boundary layer thickness of approximately 0.25 m. The freestream velocity in the wind tunnel before the bump was 10 m s^{-1}. The external flow velocity at the measurement location was found to be about 11.7 m s^{-1}. The Reynolds number based on momentum thickness ($Re_\theta = U_e\theta/\nu$, where U_e, θ and ν denote external velocity, momentum thickness and kinematic viscosity respectively) was higher than 17 000 at the measurement location. A cartesian coordinate system was used in the wind tunnel; hence x, y, z denote streamwise, wall-normal and spanwise directions.

A hot-wire rake of 143 single wire probes was used to measure the turbulent boundary layer. The rake was, as shown in Fig. 3, designed to get both temporal and spatial information about the flow simultaneously at each probe locations. Laboratoire d'Etudes Aéroydnamiques, Poitiers, France manufactured the rake, which consisted of 13 vertical comb made of double sided conventional circuit boards. Each vertical comb carried 11 single wire hot-wire sensors spaced logarithmically from wall to external flow in the wall-normal direction at wall normal positions (y) of 0.3 mm, 0.9 mm, 2.1 mm, 4.5 mm, 9.3 mm, 18.9 mm, 38.1 mm, 76.5 mm, 153.3 mm, 230.1 and 306.9 mm. The vertical combs were placed symmetrically around the centerline of the tunnel in the spanwise direction at spanwise positions (z) of 0, $\pm$4 mm, $\pm$12 mm, $\pm$28 mm, $\pm$60 mm, $\pm$100 mm and $\pm$140 mm . The rake covered an area of approximately 30×30 cm^2. The probes were distributed on an array in the plane normal to the flow and each hot-wire sensors was 0.5 mm in length and 2.5 μm in diameter. More details on the hot-wire rake and the probes are documented in [14].

An in-house developed hot-wire anemometry system of 144 channels was used for the measurements. Each of the anemometers was constant temperature anemometer, and was comprised of a Wheatstone bridge, output and sample-and-hold controls. The anemometer system originally was designed, manufactured and tested in the Turbulence Research Laboratory of the State University of New York at Buffalo [6, 16]. A Microstar Laboratories DAP 5400a processor was used as the data acquisition board. The sampling frequency was 30 kHz for all channels. In addition to hot-wire anemometer output voltages, tunnel temperature and tunnel dynamic pressure were sampled by the system at the same speed. The

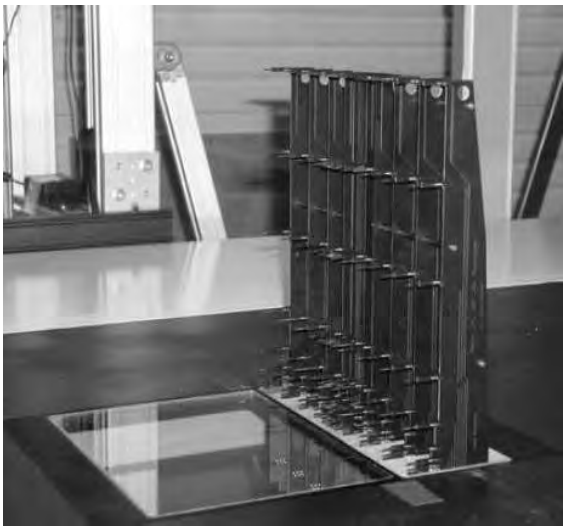

Fig. 3 Hot-wire rake in place in the LML wind tunnel.

simultaneously sampled data coming from every anemometer channels were recorded on a hard-disk for 6 seconds long blocks. The time separation, which allowed to transfer the data from buffer to the disk, was long enough to have statistically uncorrelated blocks. The details of the anemometers system also is available in [14].

Because of the mechanical design of the rake and limitation imposed by it, calibration of the hot-wire rake in a conventional way was not possible in this experiment. Therefore, we had to calibrate the wires while the probes were inside the turbulent boundary layer when the rake was in place in the test section. A new calibration method has been developed during the course of this project to perform hot-wire calibration in this kind of situations [15]. The method requires a reference mean velocity and higher order turbulence statistics at each probe locations at only one freestream velocity. In this experiment, a synchronized stereo PIV systems were used 1 cm upstream of the hot-wire rake probes, so that we obtained the required statistical data on the velocity field from the PIV measurement. This *in situ* calibration methodology together with its limitation and advantages are documented in [15].

3 Two-Point Correlations

3.1 Computation of Two-Point Correlations

Computation of two-point correlations can be summarized from [14] as follows. In a cartesian coordinate system, the two-point cross-correlation tensor writes:

$$R_{i,j}(x,x',y,y',z,z',t,t') = \langle u_i(x,y,z,t)u_j(x',y',z',t')\rangle \quad (1)$$

where the subscripts i and j represent different components of turbulent fluctuations (u, v, w). $\langle\,\rangle$ represents the ensemble average, and $'$ sign denotes different spatial positions in x, y, z coordinates and a different time. Due to stationary in time, and homogeneity in space in the spanwise direction, the two-point cross-correlation tensor given in equation (1) is only a function of separation in these coordinates. Denoting $\tau = t' - t$ and $\Delta z = z' - z$. Equation (1) can be rewritten as follows:

$$\widetilde{R}_{i,j}(x,x',y,y',\Delta z,\tau) = \langle u_i(x,y,z,t)u_j(x',y',z+\Delta z,t+\tau)\rangle \quad (2)$$

Two-point cross-spectral tensor can be obtained by performing Fourier transformation of the two-point cross-correlation in τ:

$$S_{i,j}(x,x',y,y',\Delta z,f) = \int_{-\infty}^{\infty} \widetilde{R}_{i,j}(x,x',y,y',\Delta z,\tau)e^{-i2\pi f\tau}d\tau \quad (3)$$

where f is the frequency. Since only one downstream location is considered in this study, $x = x'$ in equation (3) becomes a parameter. Therefore, equation (3) reduces to:

$$S_{i,j}(x,y,y',\Delta z,f) = \int_{-\infty}^{\infty} \widetilde{R}_{i,j}(x,y,y',\Delta z,\tau)e^{-i2\pi f\tau}d\tau \quad (4)$$

In this experiment we only measured streamwise component of the turbulent velocity, therefore the subscripts i and j are replaced by 1 and

1. The parameter x dependence in our formulation is also omitted for simplicity in the following parts of the paper.

The analysis technique can be listed as follows:

(i) Instantaneous streamwise velocities were measured at 143 point simultaneously by the hot-wire rake. As detailed in [15], the fluctuating parts of the velocity signal were obtained by subtracting the mean velocity computed over total number of measured blocks of data.

(ii) Fourier transformation of fluctuating velocity signals was performed in time for finite size record length:

$$\hat{u}(y,z,f) = \int_0^T u(y,z,t)e^{-i2\pi ft}dt \quad (5)$$

where T is the record length for each block of data taken into Fourier transformation. The total number of samples taken into FFT was 131 072 ($=2^{17}$) because of computational efficiency.

(iii) These steps were repeated for all possible configuration ($143^2 = 20\,449$).

(iv) Ensemble (block) averaged two-point spectral estimates were computed:

$$S_{1,1}(y,y',z,z',f) = \frac{\langle \hat{u}(y,z,f)\hat{u}^*(y',z',f)\rangle}{T} \quad (6)$$

where $\langle\ \rangle$ and * represent the ensemble averaging and complex conjugate respectively.

(v) Inverse Fourier transformation was used to obtain the two-point cross-correlation in physical space:

$$R_{1,1}(y,y',z,z',\tau) = \int_{-T/2}^{T/2} S_{1,1}(y,y',z,z',f)e^{i2\pi f\tau}df \quad (7)$$

(vi) The two-point correlations with separation Δx in the streamwise coordinate were computed by means of Taylor's frozen field hypothesis:

$$R_{1,1}(\Delta x,y,y',z,z') = \quad (8)$$
$$R_{1,1}(y,y',z,z',\tau = -\Delta x/U_c) \quad (9)$$

where U_c is the convection velocity. In this study we took local mean velocity as the convecting flow velocity, which is a good approximation in turbulent boundary layers [11].

3.2 Two-Point Correlation Maps

In this section we present the two-point correlations maps of the streamwise velocity fluctuation on first streamwise – spanwise (XZ) plane (which is always parallel to the wall), and second streamwise – wall-normal (XY) plane (which is always normal to the wall and freestream direction). The streamwise – spanwise correlations were obtained at constant wall-normal positions where $y = y'$. The streamwise – wall-normal correlations were computed when $z = z' = 0$. These results are grouped according to the planes they were computed and presented in Figs. 4 and 5 for XZ – and XY – planes respectively. The reference probe used in the computation of correlations were always located on the center of the rake in the spanwise direction, where $z = 0$. The other probes on which the correlation computations based were distributed on either a line parallel to the wall at constant wall-normal positions or at different wall-normal position on line perpendicular to the wall. To be able to compare current results on the APG turbulent boundary layer with the results documented in [14] for flat plate turbulent boundary layer, here we present the correlations in their normalized form using the peak founded on each plane. The peak corresponds to the two-point correlation when the separations in time and space are both zero.

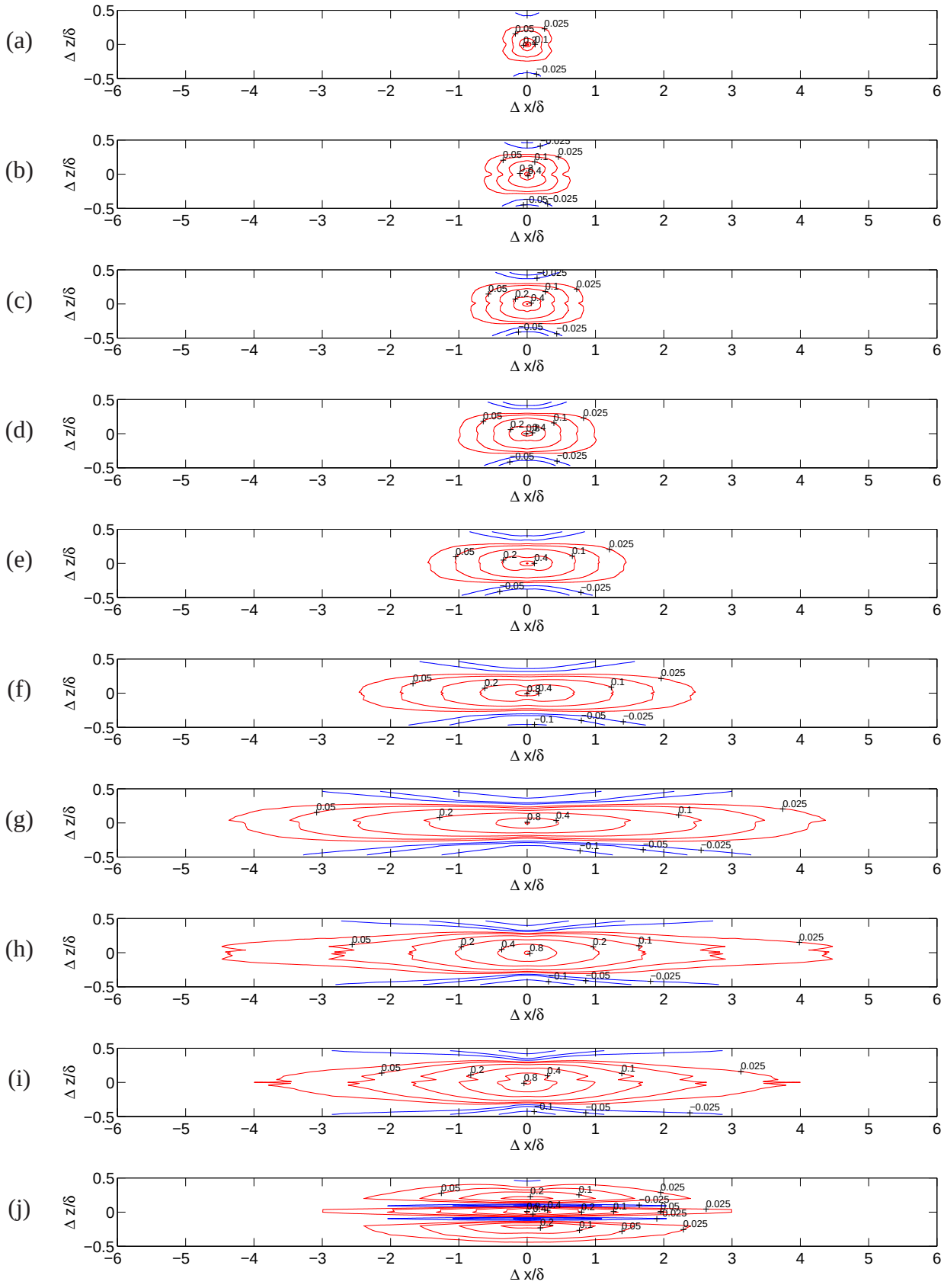

Fig. 4 Two-point cross-correlation coefficients (XZ-plane) at constant wall-normal positions. The figures present the correlations between the probe located at z=0 and the probes at the same y^+ location on each plane. y^+= (a) 6, (b) 15, (c) 32, (d) 70, (e) 145, (f) 290, (g) 590, (h) 1180, (i) 2363, (j) 3550.

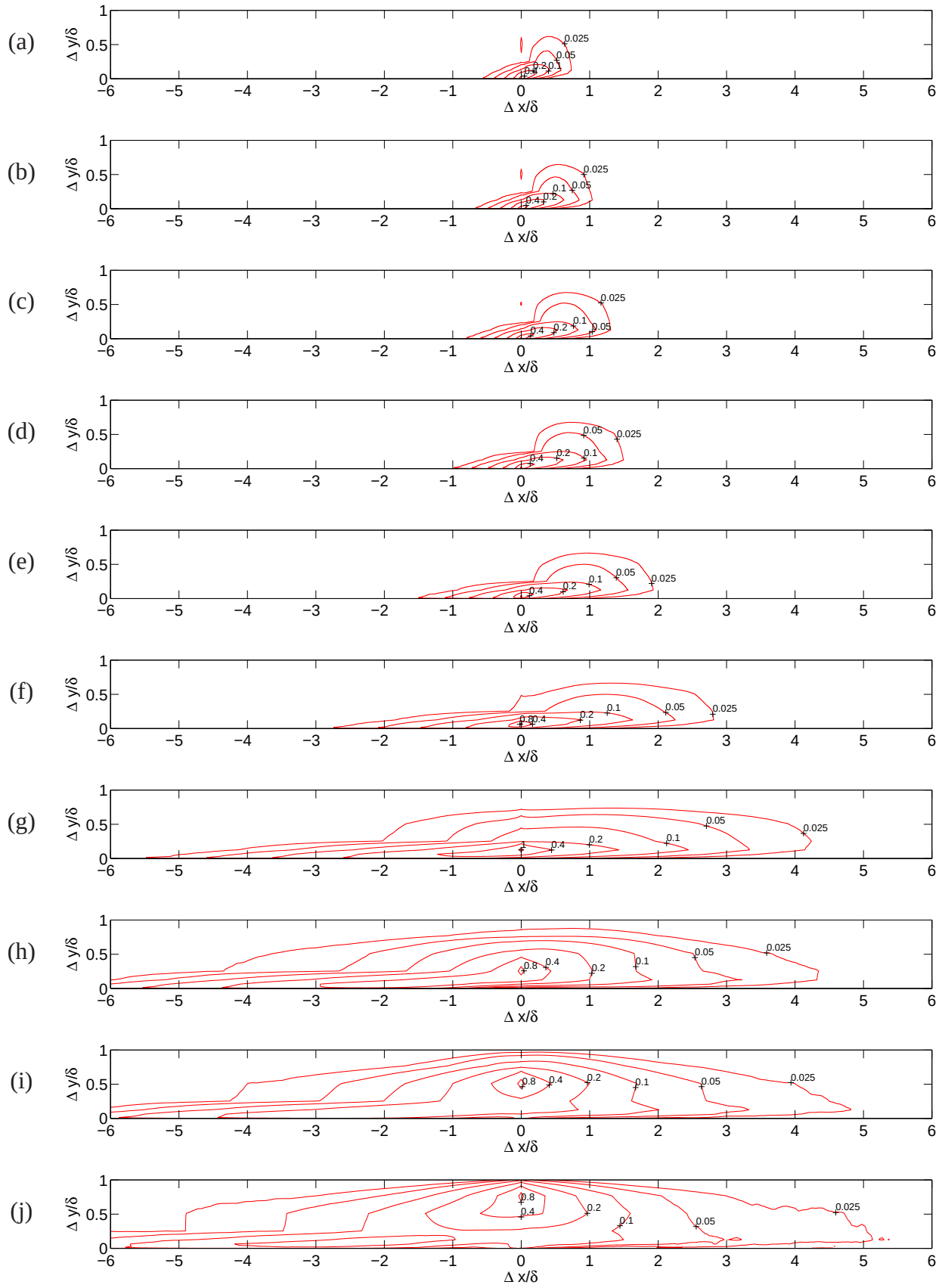

Fig. 5 Two-point cross-correlations (XY-plane) at z=0. The figures present the correlation between the reference probe at one wall-normal position, y, and the rest the probes at the same spanwise location at different wall-normal positions, y'. y^+= (a) 6, (b) 15, (c) 32, (d) 70, (e) 145, (f) 290, (g) 590, (h) 1180, (i) 2363, (j) 3550.

Fig. 4 presents the two-point correlation coefficients on the XZ planes from wall to freestream in an ascending order from (a) to (j). Separations in the streamwise direction (Δx) and spanwise direction (Δz) are normalized by the boundary layer thickness, δ, as shown in the labels of x and y axes of each figure. As mentioned earlier, the figures show the two-point correlation coefficients and the peak of each subfigure, which is one, is found at $\Delta x/\delta = \Delta z/\delta = 0$. Therefore, relative magnitude of the correlations on different y^+ locations should be assessed using Fig. 6, where lines are measured two-point correlations at corresponding y^+ locations.

As shown in Fig. 4(a) at y^+ of 6, the physical length of the area where we observe correlations is bounded between approximately $\pm 0.25\delta$ in both streamwise and spanwise directions. As the plane moves away from the wall, streamwise extent of the correlations, in particular the positive ones represented by the red contour lines, change rapidly while the spanwise extent of the correlations stays almost constant. This statement is especially true for the positive correlations. At the second plane closest to the wall, placed at y^+ of 15 shown in Fig. 4(b), length of the positive correlations in the streamwise direction, bounded between $\pm 0.6\delta$, is almost 2.5 times that at y^+ of 6. Length of the positively correlated area grows steadily from y^+ of 15 to y^+ of 145. On the other hand, the growth of the positive correlations in the streamwise direction almost doubles from y^+ of 145 to 290 and y^+ of 290 to 590. The correlation length found at y^+ of 590 is almost the maximum streamwise length observed in this experiment. The substantial increase in the length of positive correlation in the streamwise direction occur within the logarithmic region of the mean velocity profile, which was between approximately y^+ of 150 and 700. This can partly be attributed to a large increase in local mean velocity in the logarithmic layer, which then was used to compute correlations using Taylor's frozen field hypothesis. Once the XZ – plane is in the outer layer, or the so-called wake region, size of the correlations in the streamwise direction decreases constantly. At the highest wall-normal position, y^+ of 3550, presented in Fig. 4(j), we observe a sign change of correlation coefficients in the the spanwise direction, as shown by blue contour lines.

The field occupied by negatively correlated events indicated by blue contour lines is small part of the measurement window we have in the spanwise direction. Spanwise extent of the correlation contours grows very slowly from wall to top of the logarithmic layer, where it reaches at its maximum size at y^+ of 590. We observe a growth of streamwise extent of negative correlations on XZ – plane in a similar fashion that observed for positive correlations on the same planes. The maximum size of the correlation contour maps is about 6δ and are found on XZ – plane is at y^+ of 590. After this wall-normal position the physical length of the negative correlations decreases in both streamwise and spanwise directions, and almost disappears at y^+ of 3550, shown in Fig. 4(j). As mentioned previously, negative correlations at this wall-normal position appear around the center of the positively correlated region instead of both sides of the measurement window in the spanwise direction.

The shapes of the two-point correlations on the XZ – plane presented at different wall-normal positions in Fig. 4 are similar to the two-point correlations of flat plate turbulent boundary layer measured at the same facility [14]. The main difference is the streamwise extend of the correlations, which is larger in the APG case. Another difference which should be noted is related to the negative correlations, which seem to be stronger and starting from very near the wall in the APG case. In flat plate case, negative correlations are never observed around the center of the field (corresponding to vicinity of $\Delta x = \Delta z = 0$, whereas we observe negative correlations around the center for the APG case as shown in Fig. 4(j).

The two-point correlation coefficients on the XY – plane are shown in Fig. 5. The subfigures are ordered according to location of the reference probe (y) from wall to freestream in an ascending order. First we do not observe any negative two-point correlations on this plane regardless of the location of reference probe. This agrees with

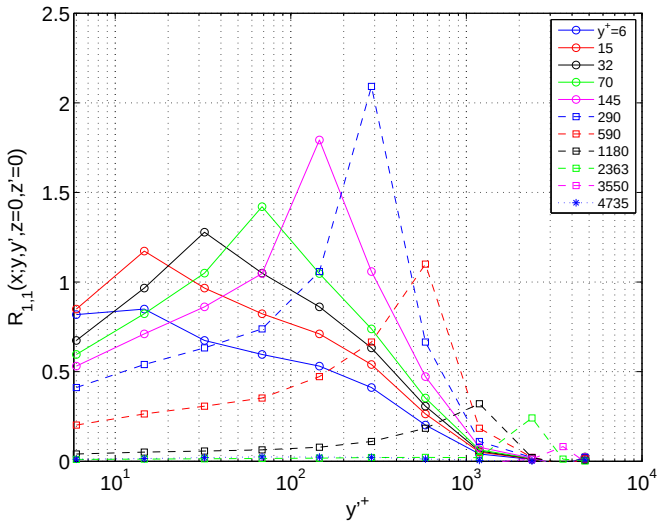

Fig. 6 Measured two-point correlation values, $R_{1,1}(x,y,y',z=0,z'=0)$, at $Re_\theta=17\,100$. Note that each curve represents the two-point correlation where reference probe is located at wall-normal position, y, while the other probes are placed at y'. Peaks found on each curve equal to the variance of turbulence at the probe location.

our previous findings on the flat plate case [14]. The maximum extent of the correlation contour lines in the wall-normal direction is fairly constant from wall to the top of logarithmic layer as shown in Figs. 5(a)–(g). After y^+ of 590, we find further development of the correlations in the wall-normal direction. As the reference probe moves away from the wall, larger areas are seen to be covered by the correlated events. Elongated correlations in the streamwise direction are especially present within the logarithmic layer and its size is on the order of 10δ. This is slightly larger than the maximum size of two-point correlations documented for flat plate case, which is about 6-7δ. The two-point correlations in the wake region shown in Figs. 5(h)-(j) show that the entire boundary layer is covered with correlated turbulent fluctuations.

In Figs. 4 and 5, the correlation coefficients are presented, so that the maximum value on each contour map is 1. Therefore, it is useful to look at Fig. 6 to measure relative strength of the correlations found on each plane or wall-normal location. It should be noted that peak of each curve shown in Fig. 6 is the value used for normalizing the two-point correlations at different wall-normal positions. These peaks indeed form a profile of variance of turbulence fluctuations in the boundary layer. An evaluation of the two-point correlation coefficients in connection with Fig. 6 indicates that a strong interaction between near wall and top of the logarithmic layer is present and produces significant correlation. Once the flow is in the outer layer, the magnitude of the correlation decreases rapidly.

4 Conclusion

In this paper, the two-point correlation of a high Reynolds number adverse pressure gradient turbulent boundary layer are documented. The database created using a hot-wire rake of 143 simultaneously sampling single wire probes were used to compute the correlations. Our analysis therefore is based only on streamwise velocity fluctuations. Computed two-point correlations using the database show that streamwise extent of the correlated events can be on the order of 10δ. The size and magnitude of the correlations are found to be increasing rapidly in the logarithmic layer. The interaction from wall to the top of the logarithmic layer produces significant correlation, indicating the presence of active structures connecting these layers. In the wake region, size of the correlations on the XZ – plane decreases in the streamwise direction. The XY – plane correlations in the wake region show that it is possible to find correlations from wall to edge of the boundary layer even though its magnitude is very small. These results especially are important to understand structural characteristics of turbulent boundary layers under influence of adverse pressure gradient and useful for the numerical computations performed in a computational box.

Acknowledgments

The authors thank S. Coudert, J.-M. Foucaut and J. Kostas of Laboratoire de Mécanique de Lille, Peter B. V. Johansson (now at Volvo Aero Corp.)

and L. Jernqvist of Chalmers, and J. Delville, P. Braud and C. Fourment of Laboratoire d'Etudes Aérodynamiques for their help in the experiment. This work has been performed under the WALLTURB project. WALLTURB is funded by the CEC under the 6th framework program (CONTRACT No: AST4-CT-2005-516008). M. Tutkun acknowledges the partial support from the Center of Excellence grant from the Norwegian Research Council to the Center for Biomedical Computing.

References

[1] Adrian R. J. Hairpin vortex organization in wall turbulence. *Physics of Fluids*, Vol. 19, No 041301, pp 1–16, 2007.

[2] Bailey S. C. C and Smits A. J. Experimental investigation of the structure of large- and very large-scale motions in turbulent pipe flow. *Journal of Fluid Mechanics*, Vol. 651, pp 339–356, 2010.

[3] Balakumar B. J and Adrian R. J. Large- and very-large-scale motions in channel and boundary-layer flows. *Philosophical Transactions of the Royal Society A*, Vol. 365, pp 665–681, 2007.

[4] Bernard A, Foucaut J.-M, Dupont P, and Stanislas M. Decelerating boundary layer: A new scaling and mixing length model. *AIAA Journal*, Vol. 41, pp 248–255, 2003.

[5] Carlier J and Stanislas M. Experimental study of eddy structures in a turbulent boundary layer using particle image velocimetry. *Journal of Fluid Mechanics*, Vol. 535, pp 143–188, 2005.

[6] Citriniti J. H, Taulbee K. D, Woodward S. H, and George W. K. Design of multiple channel hot wire anemometers. *Proc Fluid Mechanics and Instrumentation*, Vol. 183, pp 67–73. ASME-FED, 1994.

[7] del Álamo J. C and Jimenez J. Spectra of the very large anisotropic scales in turbulent channels. *Physics of Fluids*, Vol. 15, No 6, pp L41–L44, 2003.

[8] Guala M, Hommema S. E, and Adrian R. J. Large-scale and very-large-scale motions in turbulent pipe flow. *Journal of Fluid Mechanics*, Vol. 554, pp 521–542, 2006.

[9] Hutchins N and Marusic I. Evidence of very long meandering features in the logarithmic region of turbulent boundary layers. *Journal of Fluid Mechanics*, Vol. 579, pp 1–28, 2007.

[10] Kim K. C and Adrian R. J. Very large-scale motion in the outer layer. *Physics of Fluids*, Vol. 11, No 2, pp 417–422, 1999.

[11] Krogstad P. Å, Kaspersen J. H, and Rimestad S. Convection velocities in a turbulent boundary layer. *Physics of Fluids*, Vol. 10, No 4, pp 949–957, 1998.

[12] Monty J. P, Stewart J. A, Williams R. C, and Chong M. S. Large-scale features in turbulent pipe and channel flows. *Journal of Fluid Mechanics*, Vol. 589, pp 147–156, 2007.

[13] Stanislas M, Perret L, and Foucaut J.-M. Vortical structures in the turbulent boundary layer: A possible route to a universal representation. *Journal of Fluid Mechanics*, Vol. 602, pp 327–382, 2008.

[14] Tutkun M, George W. K, Delville J, Stanislas M, Johansson P. B. V, Foucaut J. M, and Coudert S. Two-point correlations in high reynolds number flat plate turbulent boundary layers. *Journal of Turbulence*, Vol. 10, No 21, pp 1–23, 2009.

[15] Tutkun M, George W. K, Foucaut J. M, Coudert S, Stanislas M, and Delville J. In situ calibration of hot wire probes in turbulent flows. *Experiments in Fluids*, Vol. 46, No 4, pp 617–629, 2009.

[16] Woodward S. H. *Progress Toward Massively Parallel Thermal Anemometry System*. M.Sc. Thesis, SUNY at Buffalo, 2001.

Copyright Statement